Plasma Physics and Controlled Fusion, Vol. 31, No. 9, pp. 1407 to 1432, 1989
Printed in Great Britain.

0741–3335/89 $3.00 + .00
IOP Publishing Ltd. and Pergamon Press plc

SENSITIVITY OF TRANSIENT SYNCHROTRON RADIATION TO TOKAMAK PLASMA PARAMETERS

N. J. FISCH
Plasma Physics Laboratory, Princeton University, Princeton, NJ 08543, U.S.A.

and

A. H. KRITZ
Department of Physics, Hunter College, New York, NY 10021, U.S.A.

(*Received* 25 *October* 1988; *and in revised form* 28 *March* 1989)

Abstract—Synchrotron radiation from a hot plasma can give information on certain plasma parameters. The dependence on plasma parameters is particularly sensitive for the transient radiation response to a brief, deliberate, perturbation of hot plasma electrons. We investigate how such a radiation response can be used to diagnose a variety of plasma parameters in a Tokamak.

1. INTRODUCTION

BRIEF, BUT INTENSE, resonant wave heating of high energy electrons can produce in Tokamaks a transient synchrotron radiation response that is distinguishable from the steady background radiation. The object of this work is to examine the sensitivity of this radiation to a number of plasma parameters; in the event that the sensitivity to certain parameters is acute, there exists the possibility of using this response to deduce these parameters. The utility of the scheme depends, of course, on the performance relative to competing diagnostics.

We formulate the problem as follows: suppose that we introduce briefly into the plasma a narrow spectrum of waves that preferentially heats superthermal electrons. The change in the electron distribution function, particularly at high energy, is manifest in a change, or increment, in the synchrotron emission. Since the excitation is brief, the changes incurred both in the electron distribution function and the accompanying synchrotron emission are transient. Thus, the *incremental* synchrotron radiation is a two-dimensional pattern in frequency–time space. The details of this pattern are governed by plasma parameters; for example, the higher the plasma density, the faster the decay of the incremental radiation.

We will show that quite gross characteristics of the radiation response can be used to deduce the governing heating and plasma parameters. By gross characteristics, we mean those that reflect primarily the two-dimensional shape of the radiation response and that are largely insensitive to noise or calibration errors. It turns out, in fact, that the gross characteristics of the radiation are sufficient to allow simultaneous deduction of several heating and plasma parameters of interest. In other words, the radiation response is sensitive in different ways to different plasma parameters.

An example of such a radiation response is shown in Fig. 1, which, although discussed in greater detail in Section 3, is presented here to illustrate the main theme of our work. The figure depicts the incremental radiation of ordinary polarization at the second, third and fourth harmonics, plotted as a function of frequency and time, that results from electrons initially with about 175 keV of parallel energy. This initial condition corresponds to the temporary increase in energetic electrons that would result from the stimulus of brief but intense r.f. heating. Corresponding also to such a stimulus would be a temporary decrease in somewhat lower energy electrons (because of particle conservation). There is indeed an incremental radiation response to this decrement too, but for simplicity we consider here only the positive part of the incremental radiation, as though energetic electrons were just put there.

In Figs 1a, 1b and 1c, we view the radiation at angles of $-15°$, $0°$ and $+15°$ with respect to the magnetic field. When the radiation is viewed at $0°$, i.e. perpendicular to the magnetic field, there is no Doppler shift to the observed frequency. Initially, because of a relativistic mass enhancement, the energetic electrons radiate at frequencies somewhat lower than each associated harmonic; as the electrons slow down,

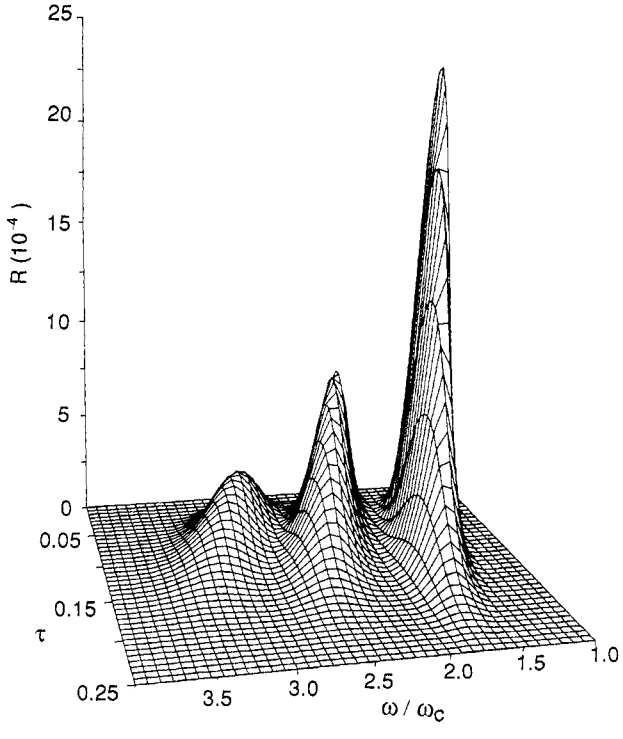

FIG. 1a.

FIG. 1.—The radiation response $R(\omega, \tau)$ for different viewing angles θ: (a) $\theta = -15°$, (b) $\theta = 0°$, (c) $\theta = +15°$. All three harmonics are apparent. In this case, it is easy to deduce the angle by just looking at the radiation response. Here, $Z_{\text{eff}} = 2$, $u_0 = 0.9$ and $\Delta u = 0.1$. Polarization is ordinary. In the plots, τ is the normalized time, i.e. $\tau = \nu_c t$, where ν_c is the collision frequency.

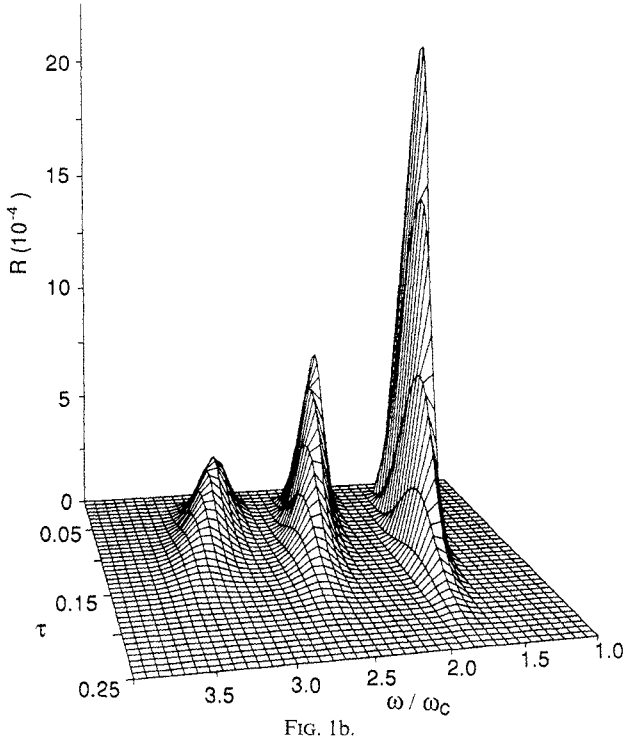
R (10⁻⁴)
20
15
10
5
0
0.05
0.15
τ
0.25
3.5
3.0
2.5
2.0
1.5
1.0
ω / ωc

FIG. 1b.

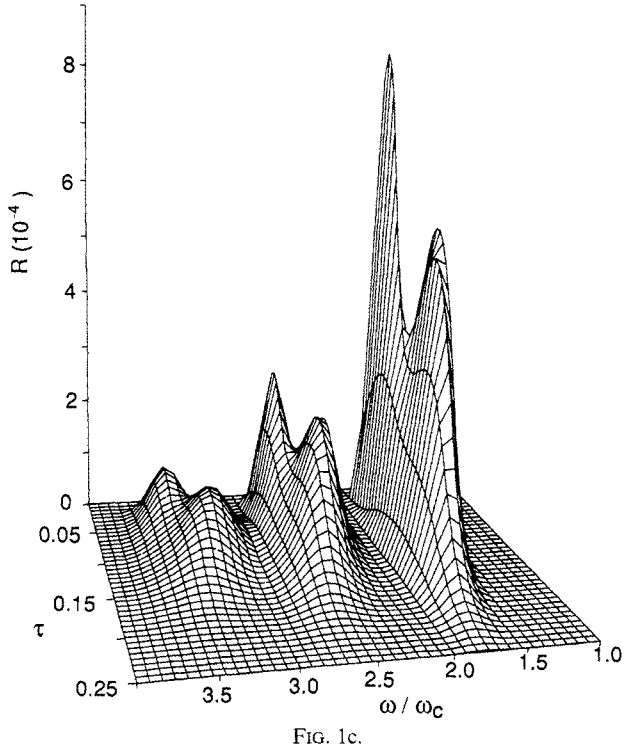
R (10⁻⁴)
8
6
4
2
0
0.05
0.15
τ
0.25
3.5
3.0
2.5
2.0
1.5
1.0
ω / ωc

FIG. 1c.

they radiate less, but at a higher frequency that approaches radiation exactly at each harmonic for completely nonrelativistic motion. When viewed at an angle with respect to the magnetic field, this picture is altered somewhat by the Doppler shift of the frequency. Note that the radiation response pictures appear quite different.

An object of this work is to see whether by observing the radiation response only, we could deduce, for example, the viewing angle. Deducing the angle of observation gives information on the direction of the magnetic field, or the q-profile, a parameter of considerble interest in Tokamak research. Other parameters of interest include the ion charge state, or, if not known, the details of the stimulus itself. In the cases of Fig. 1, it is evident that if it were only a matter of distinguishing 15° in the viewing angle, our task would be quite simple. However, more fine discriminations are of interest; in practice, what presents yet a further challenge is that the discrimination must be done in the presence of noise and, possibly, when several parameters are simultaneously unknown.

This diagnostic exploits separations of time scales: energetic electrons slow down on a collisional time scale τ_c of 10–100 ms, whereas the period of the radiation they emit $(2\pi/\omega)$ is by many orders of magnitude smaller (on the order of picoseconds); on the other hand, the response time τ_{det} of radiation detectors can be about a microsecond. Thus, we have $\omega^{-1} \ll \tau_{det} \ll \tau_c$. The first inequality suggests that there is adequate detection time to resolve finely the frequency; the second inequality suggests that it is possible to construct a diagnostic in which very many independent data points comprise the radiation response. Therefore, taking data in both time and frequency can make available perhaps several hundred data points. Such a large number of data points allows us, in using this data, to tolerate a fairly high level of noise in either the plasma or the physical detector. Actually, the experimental variables upon which the radiation response depends are likely to vary on a time scale τ_{exp} that is much longer than a collision time, i.e. $\tau_c \ll \tau_{exp}$. There would then be the opportunity to repeat many times the procedure of gathering the radiation response and to construct more statistically significant data.

In this work we restrict ourselves to the steady-state plasma (no d.c. electric field), and we identify the plasma properties that can be reliably extracted through observation of the transient radiation. The brief stimulus is assumed to result in a non-thermal electron distribution that may be taken as an initial condition. We assume that, within some range of frequencies, we can measure the pattern $R(\omega, t; \theta)$, which is the radiation emitted, at frequency ω, after time t has elapsed since the deliberate perturbation, into angle θ, where θ measures the angular deviation from purely perpendicular observation of the magnetic field. (The Tokamak is observed in the vertical plane that includes the tangent to the magnetic field **B**, so the strength of **B** may be assumed constant and known. See Fig. 2.) We consider $R(\omega, t; \theta)$ to be a two-dimensional pattern in frequency–time space, with θ (or for that matter other quantities too) entering as a parameter, possibly to be determined. The data that we choose to examine are in a frequency range such that the plasma is optically thin to the observed radiation. To evaluate this diagnostic technique, we simulated experimental data by corrupting the theoretically computed values with noise. For simplicity, we assume here that the noise is Gaussian and uncorrelated, and we then calculate the conditional probability that parameters of interest have certain values, given the noisy data.

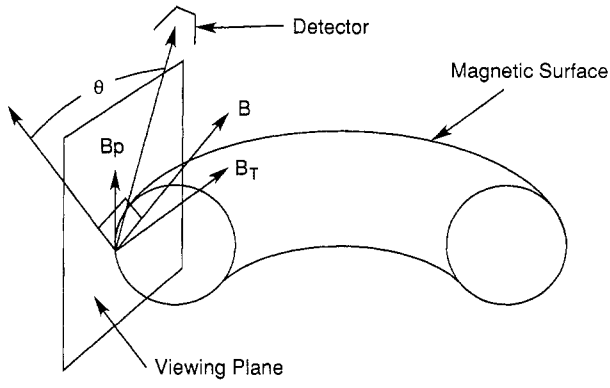

FIG. 2.—Viewing the radiation at angle θ. The viewing plane is the vertical plane that is tangent to the magnetic surface. At $\theta = 0$, the radiation is viewed perpendicular to the total (toroidal plus poloidal) magnetic field.

What emerges from our study is that even relatively high levels of noise do not prevent the simultaneous deduction to high resolution of the correct set of values for Z_{eff} (the effective ion charge state), θ (the viewing angle relative to the magnetic field), u_0 and Δu_0 (the location and width of the perturbation in velocity space). In fact, in practice, the resolution of the viewing angle, θ, is often limited instead by the divergence of the optical system (to about 1°) rather than by the level of noise. The limitation placed by the optical system means that θ and hence q on axis will be hard to resolve, although off-axis resolution to about 10% is possible. However, even if θ is not resolved very finely, the deduction of other parameters, in particular Z_{eff}, can still be accomplished. (Some ideas are given in Section 6 concerning ways of minimizing the problems associated with the optical system in deducing θ itself.)

The use of synchrotron emission to deduce plasma properties is an established and important technique. Generally, the emission is used to give information on the electron temperature; recently there have been attempts to uncover further details of the electron momentum distribution function. Useful constraints on the electron distribution function $f(p_\parallel, p_\perp)$, where $p_\parallel$ and $p_\perp$ refer to the electron momentum, respectively, parallel and perpendicular to the magnetic field, have been derived, e.g. by CELATA and BOYD (1977), TAMOR (1979), BORNATICI *et al.* (1983), CELATA (1985), HUCHINSON and KATO (1986), KATO and HUCHINSON (1986) and LUCE *et al.* (1989). In a relativistic electron ring geometry, a one-dimensional f was deduced elegantly by MAHAJAN *et al.* (1974). In these studies, the deduction of details of the electron distribution function was based on the synchrotron emission from the entire distribution of electrons; consequently, only one-dimensional data (in frequency) were used to constrain the distribution function at any particular time. Thus, while useful constraints could be derived, the available (1-D) data could not be sufficient to deduce the fully two-dimensional electron momentum distribution function, $f(p_\parallel, p_\perp)$.

The utility of information provided by transient radiation during collisional relaxation has also been recognized before: for example, ALIKAEV *et al.* (1976) observe radiation decay subsequent to intense cyclotron heating in the TM-3 Tokamak, and GIRUZZI *et al.* (1986) observe numerically the transient radiation pattern associated with cyclotron heating in the presence of a d.c. electric field. Recently, a more refined

treatment of this problem was carried out by GIRUZZI (1988), but now in the absence of a d.c. electric field.

Here, we explore the consequences of deliberately probing the plasma to produce radiation directly attributable to this probe. Obtaining in this fashion transient synchrotron emission carries, of course, the additional burden of affecting the initial perturbation. On the other hand, much more information can be gleaned from this invasive technique; in particular, the radiation pattern $R(\omega, t)$ is two dimensional, yet it gives information on variables that may be treated as independent of time. A mathematical inversion of the two-dimensional transient synchrotron data to obtain a two-dimensional electron momentum distribution function was described by FISCH (1988), assuming as given, however, other plasma parameters such as, e.g., the magnetic field **B** and the ion charge state Z_{eff}. The present work expands on the idea of using the deliberately produced transient emissions—but now for the very different purpose of uncovering spatially-resolved plasma parameters.

The paper is organized as follows: in Section 2 we derive the radiation response to an arbitrary stimulus. We specialize to the case of no d.c. electric field (steady-state plasma), for which this response can be put into a closed analytic form. This form is exceedingly fortuitous, since it allows us to easily search parameter space for the best parametric fit to given experimental data. In Section 3 we give examples of radiation patterns for different parameters and excitations. These examples, of which Fig. 1 is the first such, serve to demonstrate the basic motivation for our problem—that in the absence of noise, small changes in certain parameters produce very different looking radiation patterns. We are motivated then to examine whether this perceived sensitivity to the parameters in which we are interested is robust to noise.

In Section 4 we put forth a specific model for the noise and formulate the problem of deducing the parameters given noisy data in terms of Bayes's theorem. In other words, given the *a priori* expectation of values for our parameters in the absence of the transient synchrotron data, we deduce the *a posteriori* probabilities of values given the noisy data. In Section 5 we numerically simulate experimental noise to examine our ability to recover parameters governing the radiation response from a radiation response that is polluted by the simulated noise. Here we present the major results of this work—namely, the joint probability distributions of parameters of interest.

The figures presented in Section 5 identify those parameters which are deducible through the transient radiation. The limitations on the method with respect to deducing a q-profile are discussed in Section 6. In Section 7 we summarize our work and review in greater depth why an inquiry into the radiation of very fast electrons is well-founded. We present, too, our thoughts for further research.

2. DERIVATION OF THE RADIATION RESPONSE

Suppose that f describes the electron momentum distribution function; then the total radiation emitted from the plasma into angle θ may be written as

$$R_{\text{tot}}(\omega, \tau; \theta) = \int \mathrm{d}^3 p f(\mathbf{p}, \tau) I(\omega, \mathbf{u}; \theta). \tag{2.1}$$

Here I is the radiation power at frequency ω, due to a single electron at momentum

p, which is radiated into angle θ with respect to the magnetic field. While kept general for the moment, I will represent either the ordinary or extraordinary wave polarization. We can define an incremental or transient radiation $R(\omega, \tau; \theta) = R_{\text{tot}}(\omega, \tau; \theta) - R_{\text{back}}(\omega, \tau; \theta)$, where R_{back} is the background radiation associated with a relatively constant distribution function and R is the incremental radiation specifically due to an externally imposed impulsive momentum-space flux $\mathbf{\Gamma}(\mathbf{p}, t)$. We can then write the distribution function f as $f = f_{\text{M}}(1 + \phi_{\text{B}} + \phi)$, where f_{M} is a Maxwellian distribution, ϕ_{B} describes the relatively constant deviation from Maxwellian of the background distribution, and ϕ describes the time-dependent distribution specifically associated with the source $\mathbf{\Gamma}$. For problems of interest, in terms of contributing to the collision integral, both ϕ_{B} and ϕ may be treated as small, so that f obeys the linearized Fokker–Planck equation. The evolution of ϕ may then be written as

$$f_{\text{M}} \partial\phi/\partial t - C(\phi) = -\nabla_{\text{p}} \cdot \mathbf{\Gamma}(\mathbf{p}, t) \equiv -\delta(t) \nabla_{\text{p}} \cdot \mathbf{S}(\mathbf{p}), \tag{2.2}$$

where C is a collision term and steady state (no d.c. electric field) has been assumed. Here, the source Γ is taken to be an impulse; the physical picture is that essentially at $t = 0$ electrons are displaced in the direction of the velocity-space flux **S**. For example, were the brief stimulus to consist of an impulse of a narrow spectrum of high-phase-velocity lower-hybrid waves, then $\mathbf{S}(\mathbf{p})$ would point in the parallel direction and would be finite in a narrow range of superthermal **p**. The incremental radiation due to $\mathbf{\Gamma}$ may be written for an optically thin plasma as

$$R(\omega, \tau; \theta) = \int \mathrm{d}^3 p \, f_{\text{M}} \phi(\mathbf{p}, \tau) I(\omega, \mathbf{u}; \theta), \tag{2.3}$$

where we employ normalized momentum, $\mathbf{u} = \mathbf{p}/mc$, and normalized time, $\tau = \nu_{\text{c}} t$, with collision frequency $\nu_{\text{c}} = nq^4 \log \Lambda / 4\pi m^2 \varepsilon_0^2 c^3$. We intend to solve equation (2.2) for a variety of driving terms Γ; since we may not be entirely certain of the details of the imposed flux, we define a Green's function ψ for the radiation response, and instead write

$$R(\omega, \tau; \theta) = \int \mathrm{d}^3 u \psi(\omega, \mathbf{u}, \tau; \theta) Q(\mathbf{u}), \tag{2.4}$$

where we defined $Q(\mathbf{u}) \equiv -(mc)^3 \nabla_{\text{p}} \cdot \mathbf{S}(\mathbf{p})$. Now we need solve only an adjoint equation for ψ independent of the imposed flux, and then we obtain the radiation response by the simple integration in equation (2.4). This represents a large saving in effort if the Fokker–Planck equation (2.2) is to be solved numerically. Here, we consider the steady-state case ($E = 0$), for which an analytic solution of either the Fokker–Planck equation or the adjoint equation is possible. This solution has been given previously (Fisch, 1988), and we reiterate here the main steps.

The Green's function for the radiation response, ψ, solves the relativistic Fokker–Planck adjoint equation (see, e.g., Fisch, 1987), written for superthermal excitation in the high-velocity limit and for $E = 0$ as

$$\frac{\partial\psi}{\partial\tau}+\frac{1}{u^3}\left(\gamma^2 u\frac{\partial\psi}{\partial u}-\gamma\frac{1+Z_{\text{eff}}}{2}\frac{\partial}{\partial\mu}(1-\mu^2)\frac{\partial}{\partial\mu}\psi\right)=0, \tag{2.5}$$

with the initial condition $\psi(\omega, \mathbf{u}; \theta, \tau = 0) = I(\omega, \mathbf{u}; \theta)$, where Z_{eff} is the ion charge state and we defined $\gamma^2(u) \equiv 1+u^2$ and $\mu \equiv p_\parallel/p$. We are fortunate that this equation is tractable analytically. Separate ψ and the initial condition into Legendre harmonics, ψ_k and I_k, and the resulting equations for the ψ_k may be integrated along characteristics to obtain

$$\psi_k(\omega, u, \tau; \theta) = I_k(\omega, \rho; \theta)\left[\frac{\rho}{u}\left(\frac{\gamma(u)+1}{\gamma(\rho)+1}\right)\right]^{\alpha_k}, \tag{2.6}$$

where the characteristic $\rho(u, \tau)$ solves $G(\rho) = G(u)-\tau$, where

$$G(u) = \int_0^u (x^2/(1+x^2))\,\mathrm{d}x = u-\tan^{-1}u,$$

and where $\alpha_k \equiv (1+Z_{\text{eff}})k(k+1)/2$. For u nonrelativistic, $\rho \to (u^3-3\tau)^{1/3}$, indicating that after a time $\tau = u^3/3$, electrons initially with speed u have slowed down to $u = 0$, at which point they no longer radiate. Note that equation (2.5) is derived rigorously for superthermal u only; however, because the radiation from slowed-down less energetic electrons is small (comparable to the bulk electron emissions), for the purposes of calculating the incremental radiation, we can take equation (2.5) as universally valid.

We substitute for ψ into equation (2.4), we denote the Legendre components of $Q(\mathbf{u})$ by $Q_k(u)$, and we perform the μ-integration to get

$$R(\omega, \tau; \theta) = \sum_k \frac{4\pi}{2k+1}\int_0^\infty u^2\,\mathrm{d}u\psi_k(\omega, u, \tau; \theta)Q_k(u). \tag{2.7}$$

This is a convenient form of the 2-D response pattern, $R(\omega, \tau; \theta)$, and Fig. 1 displays such a pattern. It is presumed that this pattern is given as data; it is then our task to discover for what parameters this pattern is most likely the result. For example, note that the viewing angle θ enters parametrically; were it unknown, we would hope to deduce it—particularly so if the right-hand side of equation (2.7) were very sensitive to it. Here, we have explicitly written the parametric dependence of R upon θ, although, in fact, there are other quantities upon which R might be thought to depend parametrically, such as the ion charge state Z_{eff} (which enters through ψ), or the details of the imposed flux (which enter through Q). In practice, all of these dependencies are rather easily deduced in the absence of noise; it is the sensitivity of the deduction in the presence of noise that is our major concern.

3. DESCRIPTION OF THE RADIATION RESPONSE

Simultaneously varying several plasma parameters, we have examined the pattern $R(\omega, \tau)$. Since the responses do look different for different parameter sets, we are

motivated to uncover the parameters that govern these differences even in the presence of noise. Here, we describe in greater detail the radiation response and the model that we adopted for the stimulus to this response.

Throughout this paper, we consider the stimulus Q to be of the form

$$Q(u) \sim \exp\left[-\frac{(u\mu - u_0)^2 + u^2(1-\mu^2)}{\Delta u^2}\right], \tag{3.1}$$

which corresponds to the initial presence of a group of energetic electrons in a narrow range Δu about the parallel momentum u_0, and with little perpendicular momentum. Thus, the stimulation of the plasma is characterized by just the two parameters u_0 and Δu. Such a stimulus might arise during brief resonant heating by electrostatic waves such as lower-hybrid waves. These waves would cause an increase in the parallel energy of electrons already superthermal in the parallel direction. As discussed in reference to Fig. 1, we neglect for simplicity here the temporary decrease in the number of electrons with somewhat lower energy—the inclusion of that effect would increase the amount of information available and so would lead to a more precise deduction of the governing parameters, but that is an embellishment that we can postpone. Although we have some control over the launching and damping of the lower-hybrid wave, we may still be unsure as to the precise details of the damping. Hence, we do not consider the parameters u_0 and Δu necessarily as given or known.

In Fig. 1 we showed the radiation response to such a stimulus. Note that the radiation response first rises and then falls, all the while being shifted to higher frequencies. The reason for this behavior is that for a narrow excitation (Δu small), the incremental electrons initially have parallel energy but little perpendicular energy. Since cyclotron radiation arises from perpendicular motion, initially there is very little radiation. Due to collisions, however, these electrons are pitch-angle scattered so that their parallel energy is converted to perpendicular energy. Therefore, within a pitch-angle scattering time, there is a great increase in the incremental radiation. On the other hand, the slowing-down time of these electrons due to energy scatters is comparable to the pitch-angle scattering time. When the electrons slow down they radiate less. Moreover, as they become less relativistic, the frequency of the radiation is downshifted less, so the electrons radiate at the nonrelativistic harmonics. In Fig. 1, we depict the second, third and fourth harmonic radiation; note that in time the spectrum tends to higher frequency, and by the time all of the initially disturbed electrons slow down, what little remains of the radiation is at each of the harmonics. (To obtain, from the radiation response in Fig. 1, the power in erg $\sec^{-1}$ per unit frequency per radiating electron viewed by the detector, multiply R by $e^2\omega^2/c$, where e is the electron charge in statvolts and c is the velocity of light.)

The radiation patterns will differ somewhat depending upon the polarization observed. The radiation intensity, for ordinary polarization (i.e. with **E** vector parallel to the magnetic field) may be written as (see, e.g., LANDAU and LIFSHITZ, 1951)

$$I^{O}(\omega, \theta, \mathbf{u}) = \sum_n \frac{e^2\omega^2}{2\pi c\lambda^2}\left(\frac{\sin\theta - u\mu/\gamma}{\cos\theta}\right)^2 J_n^2\left(n\frac{u}{\gamma}(1-\mu^2)^{1/2}\frac{\cos\theta}{\lambda}\right)\delta(\omega - n\omega_c/\gamma\lambda), \tag{3.2}$$

where n is the cyclotron harmonic, J_n is the n-th Bessel function of the first kind, $\omega_c = eB/mc$ is the cyclotron frequency of nonrelativistic electrons, and $\lambda = 1 - u\mu \sin\theta/\gamma$ is the extent of the Doppler shift through viewing the radiation at angle θ. The radiation intensity at the extraordinary polarization may be written as

$$I^X(\omega, \theta, \mathbf{u}) = \sum_n \frac{e^2\omega^2}{2\pi c\lambda^2}\left(\frac{u}{\gamma}\right)^2 (1-\mu^2) J_n'^2 \left(n\frac{u}{\gamma}(1-\mu^2)^{1/2}\frac{\cos\theta}{\lambda}\right)\delta(\omega - n\omega_c/\gamma\lambda), \quad (3.3)$$

where J_n' is the derivative of the n-th Bessel function of the first kind. Note that while in both instances of polarization the radiation vanishes for electrons with only parallel energy ($\mu^2 = 1$), the radiation at the extraordinary polarization is maximized when the electron has purely perpendicular motion ($\mu = 0$), whereas for the ordinary polarization, the radiation intensity is maximized for intermediate pitch-angle ($0 < \mu^2 < 1$). For perpendicular observation ($\theta = 0$), in fact, the ordinary wave polarization is not observed from electrons with purely perpendicular motion. Hence, the radiation plots of the ordinary wave emission show faster rise times in the radiation amplitude than do plots of the extraordinary polarization (for the kind of excitations that we consider here—electrons initially with only parallel energy), since electrons initially travelling nearly in the parallel direction need be scattered less in pitch-angle to emit at their maximum.

The parameter that governs the relative importance of pitch-angle to energy scattering is Z_{eff}. For large Z_{eff} the pitch-angle scattering occurs more quickly; the energy scattering is unaffected. A quick rise time for the radiation, but a long decay time, therefore, indicates high Z_{eff}.

The response pattern $R(\omega, \tau)$ is also sensitive to the location of the excitation $Q(\mathbf{u})$ (see Fig. 3). When high-energy electrons are affected (u_0 large), there is a strong relativistic effect that downshifts the frequency. Moreover, since high-energy electrons slow down more slowly, the incremental radiation due to these electrons persists longer. Small changes in the parameter u_0 therefore result in quite distinguishable patterns especially in the case of a relatively narrow excitation ($\Delta u \ll u_0$). For very broad excitation ($\Delta u \sim u_0$), these differences are less dramatic. On the other hand, since relativistic electrons of slightly different velocity radiate at different frequencies, when u_0 is large, it should be quite easy to surmise Δu from the frequency extent of the pattern $R(\omega, \tau)$.

The pattern $R(\omega, \tau)$ is also sensitive, as we have seen in Fig. 1, to the viewing angle θ. Viewing at finite θ uncovers the Doppler shifts which give information on both the direction of the magnetic field and the location in velocity space of the perturbed electrons. It is evident that the gross form of the radiation response differs markedly at large viewing angles. This is particularly striking for narrow stimuli ($\Delta u \ll u_0$) and when viewing for θ positive, i.e. in the direction of oncoming electrons. For such a case, in fact, the pattern $R(\omega, \tau)$ develops a two-humped structure at each harmonic, as depicted in Fig. 1c.

This curious structure of the radiation response at $\theta = 15°$, where R shows for each harmonic two maxima in time at constant ω, is not artifactual and perhaps it is worth a brief digression to explain it. Note that at each pitch-angle the emitted fre-

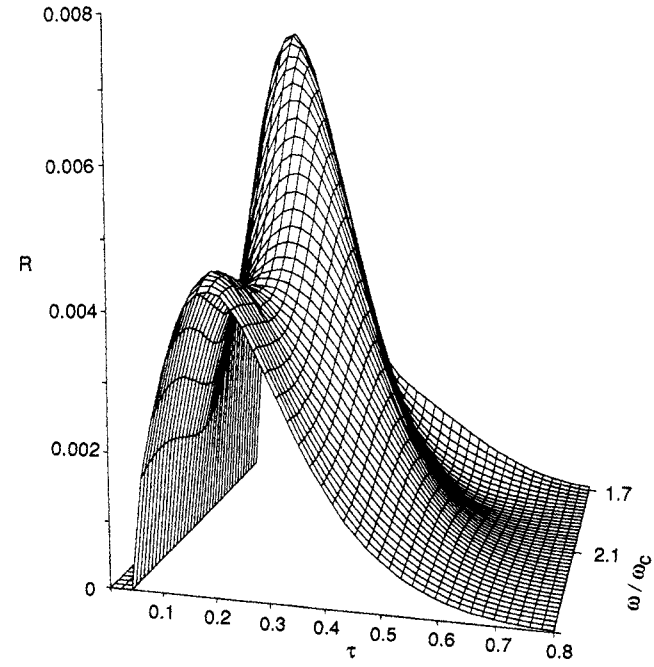

FIG. 3a

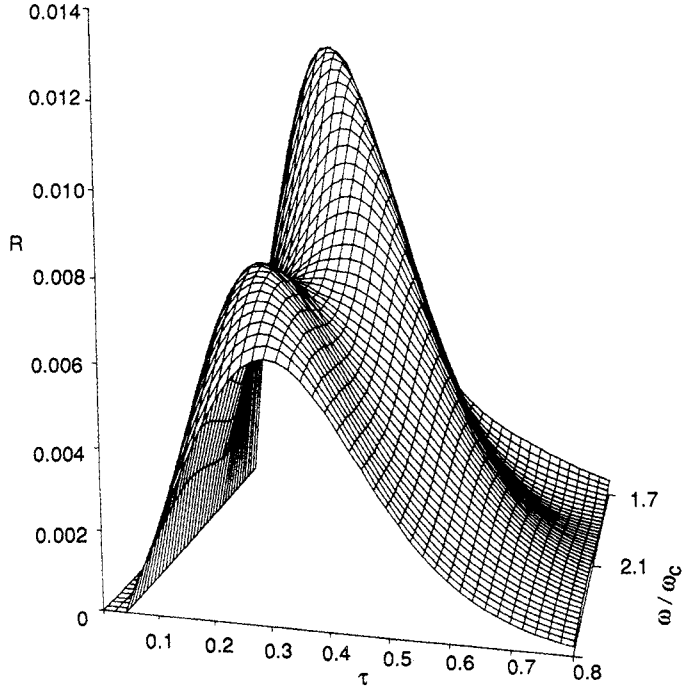

FIG. 3b

FIG. 3.—The radiation response $R(\omega,\tau)$ for different excitation location u_0: (a) $u_0 = 1.4$, (b) $u_0 = 1.6$. In both cases $\Delta u_0 = 0.3$, $Z_{\text{eff}} = 2$ and $\theta = 0$. Polarization is ordinary. Both third and fourth harmonic radiation contribute in the frequency window exhibited.

quency is $\omega = n\omega_c/\gamma\lambda$, or $u\mu/\gamma = (1-n\omega_c/\gamma\omega)/\sin\theta$, and the Doppler shift is $\lambda = 1-(u\mu/\gamma)\sin\theta = n\omega_c/\gamma\omega$. Thus, we have from equation (3.2) the proportionalities

$$I^{O} \sim (\omega^2/\lambda^2)(\sin\theta - u\mu/\gamma)^2 J_n^2 \sim [\omega^2 \sin^2\theta - (\omega - n\omega_c/\gamma)^2]^2 J_n^2. \tag{3.4}$$

Now for $\theta = 0$ precisely, $\omega = n\omega_c/\gamma$, so a spread in initial energies gives rise merely to a spread in frequency response centered about $\omega = n\omega_c/\gamma$, where $\gamma(\tau)$ decreases with time. However, for finite θ, we calculate a local minimum at $\gamma(\tau) = (n\omega_c/\omega)/\cos^2\theta$, if we neglect for the moment the Bessel function. The question is whether this local minimum is in the emitted spectrum. To check for this, note that the resonance condition gives $\gamma(\tau) = n\omega_c/\omega\lambda$, so we must have

$$\gamma(\tau) = n\omega_c/\omega\lambda = (n\omega_c/\omega)/\cos^2\theta, \tag{3.5}$$

and, using the definition of λ, this condition reduces to

$$\mu u/\gamma = \sin\theta. \tag{3.6}$$

Thus, there is the possibility of satisfying the above condition for an initial perturbation of electrons such that $\mu u/\gamma > 0$, as in our case, and for a viewing angle such that also $\sin\theta > 0$. Actually, very similar reasoning leads, for $\sin\theta > 0$, also to the possibility of two maxima in frequency at constant time, something we have also observed for single-peaked initial velocity-space perturbations of the electron distribution function, provided the ordinary mode emission is viewed at a positive viewing angle.

Of course, as electrons slow down the initial conditions become increasingly less relevant; the electrons spread in pitch-angle to cover uniformly the velocity shell rendering little different viewing from positive and negative angles. The emission decreases for the slower electrons and the distinction of the double-peaked distribution becomes less dramatic. It remains, however, that the two-peaked response is a distinguishing feature of $\theta > 0$ viewing of ordinary emission, at least for excitations relatively narrow in velocity space ($\Delta u/u_0 \ll 1$).

In the problem as we have posed it, there are only several parameters that we consider as possibly unknown: the ion charge state Z_{eff}, the viewing angle θ, and the stimulus parameters u_0 and Δu. Additionally, the plasma density, toroidal field, and the stimulus magnitude also govern the radiation response. It turns out that it is not difficult, almost by inspection merely of the radiation response, to determine what some of these parameters must be, and the parameter search, in general, may be reduced through the examination only of a judicious set of distinguishing feaures in the radiation response.

4. DEDUCTION OF PLASMA PARAMETERS IN THE PRESENCE OF NOISE

In a typical experiment, noise can arise from a variety of sources. For example, it may not be possible to subtract out entirely the radiation associated with the background plasma, especially in the vicinity of the cyclotron harmonics. A second source of noise arises from our inability to calibrate precisely a large array of radiation detectors. Moreover, there may be unwanted reflections within the plasma chamber

that interfere with the direct radiation signal. It is not our intention to construct precise models for these sources of noise; rather it is our intention to propose a generic model for noise and other unwanted effects, and then to examine how robust our deductions remain in the presence of possibly large amounts of this generic noise. It is our expectation that this robustness will not be particularly sensitive to our choice of noise model.

The noise model that we employ assumes that each attempt to measure experimentally $R(\omega, \tau)$ results in a pollution by an extraneous signal $\tilde{R}(\omega, \tau)$. Thus, we measure only

$$R_x(\omega, \tau) = R(\omega, \tau) + \tilde{R}(\omega, \tau). \tag{4.1}$$

We make the further assumption that the noise $\tilde{R}(\omega, \tau)$ is Gaussian and uncorrelated over the discrete measurements that we make; each measurement of the pattern $R(\omega, \tau)$ is corrupted by a noise $\tilde{R}$, with the properties $\langle \tilde{R} \rangle = 0$ and $\langle \tilde{R}^2 \rangle = \sigma^2$. The sensitivity of our deductions is then a function of the noise mean amplitude σ, which we assume to be constant in time and frequency. The probability density of observing experimentally at time τ and frequency ω an incremental signal of amplitude $R_x(\omega, \tau)$, given a set of plasma conditions which we denote by Θ, can then be written as

$$P[R_x(\omega, \tau) \mid \Theta] = \frac{1}{\sqrt{\pi}\sigma} \exp\left[- \frac{[R_x(\omega, \tau) - R(\omega, \tau; \Theta)]^2}{\sigma^2} \right]. \tag{4.2}$$

Suppose that we take data for some set of frequencies and times $\{\omega_i, \tau_i\}$, numbering say N_D data measurements in all. Then the probability that given some set of parameters Θ, we precisely find the whole pattern $R_x \equiv \{R_x(\omega_i, \tau_i)\}$, is given by

$$P(R_x \mid \Theta) \equiv P[\{R_x(\omega_i, \tau_i)\} \mid \Theta] = \sum_{i=1}^{N_D} P[R_x(\omega_i, \tau_i) \mid \Theta], \tag{4.3}$$

i.e. the product of the probabilities of each datum, since we have assumed that the noise is uncorrelated. If it were certain that measurements were obtained in the complete absence of noise, i.e. $\sigma \to 0$, then even one measurement $R_x(\omega_i, \tau_i)$ differing from the expected measurement $[R_x(\omega_i, \tau_i) \mid \Theta]$ for the parameter set Θ immediately rules out that parameter set Θ as possibly explaining the data. In the opposite limit of utter noise, $\sigma \to \infty$, all measurements are equally likely for any data set, so no particular set of of parameters is the preferred explanation of the data. Of course, for finite noise, there is no guarantee that *any* parameter set Θ can reproduce exactly a particular noisy observation R_x.

Given the above model for noise, we can now make precise statements concerning the sensitivity of our deductions to noise of this type. While the model for noise does make certain assumptions which are not realistic descriptions of noise in general, these assumptions are likely to serve quite well for the purposes here. For example, whereas it is likely that there will be very significant correlations in the noise—take for example some sort of jitter—for the purposes of distinguishing the particular two-dimensional patterns $R(\omega, \tau)$, these correlations are unlikely to confuse. The set of

pictures that we consider are decaying functions in time, with an unusual, continuous dependence on both frequency and time. Hence, noise of an oscillatory quality, or affecting only a few detectors, will not present signals that would be misleading in our analysis.

For the purposes of interpreting the data that make up the patterns $R(\omega, \tau)$, any noise that we might expect, e.g. miscalibration, or extraneous signals, might reasonably be modeled as uncorrelated, to the extent that the correlations that do arise do not lead us to favor any particular set of parameters $\{\Theta\}$. Of course, this is an assumption that ought to be checked. Also, in practice, better noise models exist; for example, miscalibrations might be modeled as uncorrelated in frequency but not time.

While we have characterized all noise only by the amplitude, we have left open the interpretation of what precisely that amplitude should be. To relate the results here to any particular experiment, the precise sources of noise in that experiment are to be summarized roughly as just one number, the amplitude. Exactly how this correspondence is made we do not address here; our interest is in uncovering the main, general features of the noise sensitivity. Of course, different sources of noise in different experiments are confusing to different degrees.

The problem we formulate is: given the uncertainty in our measurements due to noise, how likely is it that any particular set of parameters governs the physical process that we observe? Here we seek to obtain not only the most likely set of parmeters, but also a sense of the relative likelihood of competing sets of parameters. The precise posing of this problem requires the further specification of the *a priori* probabilities of our parameters, i.e. the expectation of these parameters in the absence of any data whatsoever. For example, in the absence of data we have certain expectations concerning the likelihood of the average ion charge state, Z_{eff}. Possibly, we may have other experimental measurements that reinforce these expectations. We take these expectations into account using a Bayesian approach. Suppose that the *a priori* probability of the parameter set $\{\Theta\}$ is given by $P(\Theta)$. Then the probability of the parameter set Θ given both the *a priori* probability of the parameter set and the set of observations R_x can be written as

$$P(\Theta \mid R_x) = \frac{P(R_x \mid \Theta) P(\Theta)}{P(R_x)}, \tag{4.4}$$

where the right-hand side of the above Bayes's theorem consists of known or calculable quantities. In particular, $P(R_x \mid \Theta)$ is given by equation (4.2) and the denominator can be written as a sum over all possible parameter sets, namely

$$P(R_x) = \sum_{\{\Theta\}} P(R_x \mid \Theta) P(\Theta). \tag{4.5}$$

In practice, $P(\Theta)$ might be obtainable from other measurements or presumed from a theory of Tokamak operation. In this work, we shall simply assume that there is uniform *a priori* probability for parameters within some range of values.

Equation (4.4) outlines the procedure applicable for reducing experimentally obtained data, resulting in the probability distribution for $P(\Theta)$. The peakedness of the resulting probability distribution is a reliable measure of the sense that can be

made of the data. It is worthwhile to inquire, however, before such data are produced, what might be their worth, or information content, were they produced. The probability distribution with which we expect to deduce the plasma parameter set $\{\Theta\}$, given that the data were obtained in the presence of noise σ and generated with the specific plasma parameter set $\{\Theta_p\}$, can be written as

$$P(\Theta|\Theta_p;\sigma) = \sum_{\{R_x\}} P(\Theta|R_x;\sigma)P(R_x|\Theta_p;\sigma), \tag{4.6}$$

where the sum is over all possible data sets $\{R_x\}$, and the summand is the probability of deducing $\{\Theta\}$ given the noisy data set times the probability that such a data set would be generated in the first place.

Clearly, $P(\Theta|\Theta_p;\sigma)$ is an important measure of information; the characteristic width of this probability distribution gives the expected sensitivity for distinguishing plasma parameters by means of the radiation response. Of course, it is infeasible to evaluate equation (4.6) through a consideration of all possible data sets; however, to find $P(\Theta|\Theta_p;\sigma)$, we can numerically generate data sets $R_x^{(j)}$ by polluting the radiation response to $\{\Theta_p\}$, as indicated in equation (4.1). We now average the probability distributions $P(\Theta|R_x^{(j)};\sigma)$ over N_R such realizations or data sets, noting the asymptotic approximation

$$P(\Theta|\Theta_p;\sigma) = \lim_{N_R\to\infty} \frac{1}{N_R} \sum_{j=1}^{N_R} P(\Theta|R_x^{(j)};\sigma). \tag{4.7}$$

Since the data sets $R_x^{(j)}$ occur, by construction, with probability $P(R_x|\Theta_p;\sigma)$, equation (4.7) is obtained in the limit of many data sets. Generally, $N_R \sim 80$ suffices to approximate $P(\Theta|\Theta_p;\sigma)$. Note, incidentally, that in equation (4.6), whereas the probability distribution $P(R_x|\Theta_p;\sigma)$ peaks at $R_x = R(\omega,\tau,\Theta_p)$, i.e. the unpolluted data are most likely, and, whereas, for $R_x = R(\omega,\tau,\Theta_p)$, the probability distribution $P(\Theta|R_x;\sigma)$ peaks at the true parameter set $\Theta = \Theta_p$, it is *not* necessarily the case that the probability distribution $P(\Theta|\Theta_p;\sigma)$ peaks at $\Theta = \Theta_p$. We do expect such peaking in the limit of zero noise, $\sigma \to 0$, and, in the opposite limit of utter noise, we expect no peak at all. However, for intermediate noise levels, although the true parameters are probably very nearly the most likely if not the most likely, there is no requirement that the peak (i.e. maximum likelihood) actually coincides with $\Theta = \Theta_p$ (even in the limit $N_R \to \infty$).

5. PROBABILITY DISTRIBUTION OF PLASMA PARAMETERS

In the absence of noise, the parameters of interest are easily deduced. In the presence of noise, we construct the joint probability distribution of unknown parameters given the data, given the *a priori* probability of the parameters, and given a level of noise that we can model as described in the previous section. Before giving examples of such joint distributions, we show in detail the construction of one such distribution.

Consider, for example, the probability $P(\theta|\theta_p;\sigma)$, which we can construct for different noise levels σ using equation (4.7). A noise level, say, $\sigma = 30\%$ corresponds to the corruption of the *true* data generated using parameter set $\theta = \theta_p$ by noise equal

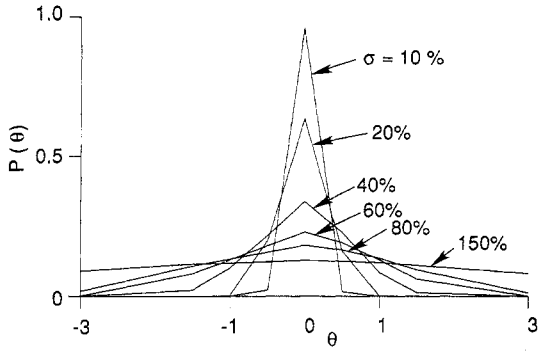

FIG. 4.—Probability $P(\theta|\theta_p = 0; \sigma)$ vs θ. Examples of one parameter probability distribution—with noise σ entering as a parameter. The noise levels plotted are 10%, 20%, 40%, 60%, 80% and 150%. True data are $\theta_p = 0$. Here, $u_0 = 0.9$, $Z_{eff} = 2$ and $\Delta u_0 = 0.1$. Polarization is ordinary. The frequency window ($1.8 < \omega/\omega_c < 3.0$) is chosen to emphasize the third harmonic. Here, $N_R = 20$ and $N_D = 1600$.

to 30% of the maximum amplitude, so that as the radiation decays, the signal/noise ratio becomes smaller. We assume for the purposes of this example that all other parameters are known, and that θ takes with equal *a priori* probability only the nine discrete values in the set $\{0.0°, \pm 0.5°, \pm 1.0°, \pm 2.0°, \pm 3.0°\}$. Suppose also that the *true* value of θ is zero—namely, $\theta_p = 0$—so that, in reality, the radiation is viewed in the purely perpendicular direction. Then the *true* radiation plot should be as given in Fig. 1b, but what we observe in an experiment, in fact, is a noise-corrupted version of this plot, simulated here by adding Gaussian, uncorrelated noise to the *true* plot, to get R_x. The noise-corrupted plot, or, more precisely, a set of such noise-corrupted plots, is then used to compute $P(\theta|\theta_p = 0; \sigma)$.

In Fig. 4 we show $P(\theta|\theta_p = 0; \sigma)$ for different noise levels σ. Here, we compare the noisy data to the data that might be expected for each of the possible angles θ. Note that in the limit of zero noise ($\sigma = 0$), the correct viewing angle is determined with certainty, i.e. $P(\theta|\theta_p = 0; \sigma) \sim \delta(\theta)$. In the opposite limit of utter noise ($\sigma \sim \infty$), all viewing angles are equally likely, i.e. $P(\theta|\theta_p = 0; \sigma) = 1/9$; in other words, the utterly noisy data are useless, so the *a priori* probabilities are left unchanged in full consideration of the data. These limiting cases are apparent in Fig. 5, where we show the

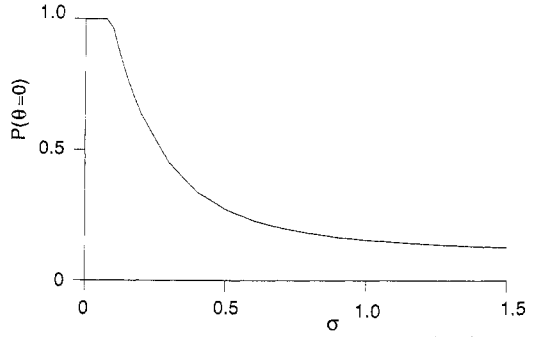

FIG. 5.—Probability $P(\theta = 0|\theta_p = 0; \sigma)$ vs σ. Parameters are as in Fig. 4. Low and high noise levels show limits, respectively, of complete and no information. There are nine cases examined for θ, so the limiting probability for utter noise is 1/9.

probability with which the correct viewing angle is deduced as a function of the noise level. [Here, in discretizing θ, we calculate finite probabilities; of course, in reality, θ is continuous, and one ought to view as significant only the shape of $P(\theta)$, which approximates the shape of the probability density.]

In constructing Fig. 4, we treated all parameters other than θ as known precisely. Using equations (4.2)–(4.5), we matched the data against the radiation responses that would be expected for each value that the unknown θ can take. The probability distribution of interest and depicted in Fig. 4 is an average of equation (4.4) over different realizations of the noisy data, as given by equation (4.7). Here, we take $N_R = 20$, and each data set is comprised of 1600 data points ($N_D = 1600$) corresponding to a 40×40 grid of measurements in ω–τ space. The grid of measurements includes a time interval just sufficient to observe the full decay of the incremental radiation, and a frequency range that emphasizes the third harmonic radiation ($1.8 < \omega/\omega_c < 3.0$). Note that for uncorrelated noise, the probability distribution depends only on the parameter combination σ^2/N_D, i.e. quadrupling the amount of data allows the same accuracy at double the noise level.

Although we treat here only one parameter (θ) as unknown, in the event that more than one parameter were unknown, we would construct the joint probability distribution of all of the unknown parameters given the data. For example, suppose that we wish to determine the viewing angle, but we are unsure as to exactly where in velocity space the impulsive heating took place—i.e. we consider u_0 as unknown. We can model the *a priori* probability distribution of u_0 as equally likely on a discrete set of values. In Fig. 6 we show the joint probability distribution for two different noise levels; again, for a low noise level, the two unknown parameters are deduced with precision. The data are generated using the parameters $(\theta, u_0) = (\theta_p, u_p)$, with $\theta_p = 0$ and $u_p = 1.5$. Note that the greatest confusion occurs for negative θ and higher u_0 or positive θ and lower u_0, since, to some extent, the relativistic frequency change is cancelled by viewing Doppler-shifted radiation. Nonetheless, the confusion is not

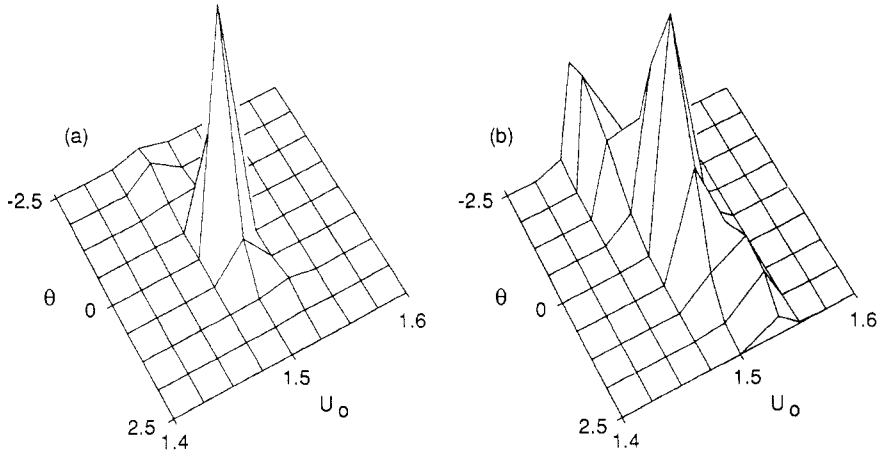

FIG. 6.—Joint probability distribution of viewing angle θ and stimulus location u_0 for two noise levels: (a) $P(\theta, u_0 | \theta_p = 0, u_p = 1.5; \sigma = 0.15)$ vs θ and u_0, (b) $P(\theta, u_0 | R_x; \sigma = 0.30)$ vs θ and u_0. Polarization is ordinary. Here, $Z_{eff} = 2$ and $\Delta u = 0.3$. The radiation is observed in the frequency window $1.7 < \omega/\omega_c < 2.5$. Here, $N_R = 80$ and $N_D = 1600$.

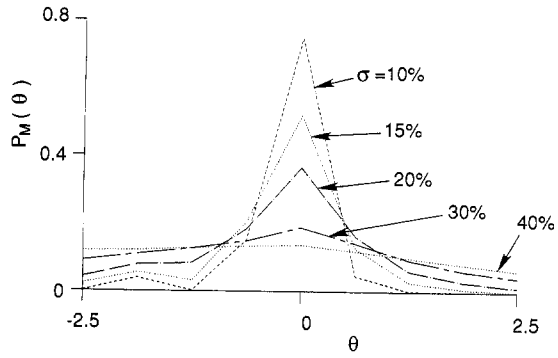

FIG. 7.—Marginal probability distribution of θ for different noise levels: derived from joint probability distribution shown in Fig. 6. The noise levels plotted are 10%, 15%, 20%, 30% and 40%.

great, since there remain other distinguishing features, such as the longer persistence of incremental radiation stimulated at higher u_0.

What is remarkable is that the precision with which either is deducible is not materially affected by our lack of knowledge of the other parameter. This we show in Fig. 7, where we plot the marginal probability distribution

$$P_M(\theta|\theta_p = 0, u_p = 1.5; \sigma) \equiv \sum_{u_0} P(\theta, u_0|\theta_p = 0, u_p = 1.5; \sigma). \tag{5.1}$$

Similarly, we show in Fig. 8 the marginal probability distribution of u_0, which exhibits quite fine resolution of u_0. (The fine resolution might have been anticipated from the large disparity in the radiation responses for nearby u_0, an example of which was presented in Fig. 3.) Note that the noise levels shown in Fig. 8 are higher than those shown in Fig. 7. The marginal distribution of u_0 might correspond to the case when we are experimentally unable to resolve finely the viewing angle.

The fact that these marginal distributions are not terribly different from the prob-

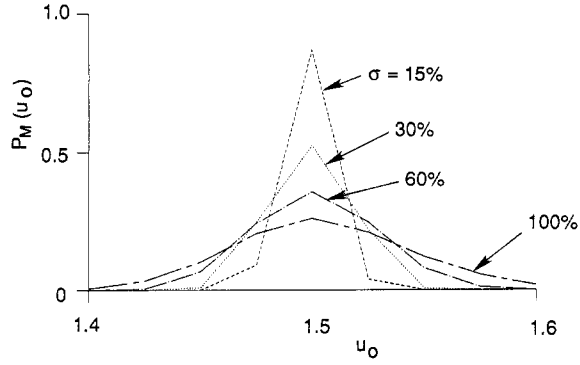

FIG. 8.—Marginal probability distribution of u_0 for different noise levels: derived from joint probability distribution shown in Fig. 6. The noise levels plotted are 15%, 30%, 60% and 100%.

ability distribution when all other parameters are assumed known indicates that the radiation response indeed depends in very different ways on the parameters of interest. This is a fortuitous occurrence that could not have been anticipated, i.e. we had no assurance that the radiation plot would not look approximately the same for very different parameter sets. (This is not to say that there are not ignorable parameters; there are parameters that simply cannot be determined, but not knowing them even approximately does not impair our deduction of other parameters.)

Although the radiation responses for different sets of parameters are distinct, it is unwieldy to consider all permutations of unknown parameters. The deductive work can be significantly reduced by what might be called *feature selection*. For example, one parameter of which we may be ignorant is the amount of r.f. power that is deposited as the stimulus, i.e. the magnitude of **S**. Here we envision that it is far easier to determine the direction and functional dependence of the induced flux than it is to determine its precise magnitude. However, while the radiation response $R(\omega, \tau)$ certainly does appear very different for different magnitudes S, the *shape* of $R(\omega,\tau)$ is invariant. Thus, the correct feature selection is to deduce parameters on the basis of only *shape* when we are interested in parameters other than the magnitude S, and when, conversely, we are entirely disinterested in the parameter S. This can be accomplished, for example, by normalizing the area under response plots for the sets of parameters that we match to the noisy data. The sense in which this represents a *feature selection* is that we expect the probability distribution $P(\Theta \mid R_x)$ for parameter set Θ that we calculate in this manner [e.g. as in equation (4.6)] to approximate the rigorously defined marginal probability distribution

$$P(\Theta \mid R_x) = \sum_S P(\Theta, S \mid R_x). \tag{5.2}$$

There is, however, a considerable saving in computation to work with normalized data rather than to consider the parameter space to have yet another dimension. In this work, in fact, we compare only normalized response plots.

Of course, one could extend this project, seeking to select other features. For example, we could try to remove the sensitivity on the placement of the excitation spectrum, i.e. u_0, by considering radiation responses to be not only shape-invariant (through normalization) but also shift-invariant in ω. Such exercises could indeed simplify the parameter search, but the process itself of feature selection is beyond the scope of the present work. Here, we seek merely to establish the sensitivity of the radiation response to plasma parameters—which is the ultimate motivation for further study of the method.

One plasma parameter of particular interest, and to which existing diagnostics are not terribly sensitive, is the ion charge state Z_{eff}. In Fig. 9 we show, for example, the joint probability distribution $P(Z_{\text{eff}}, u_0 \mid Z_{\text{p}}, u_{\text{p}}; \sigma)$ for different noise levels. The data are generated using the parameters $(Z_{\text{eff}}, u_0) = (Z_{\text{p}}, u_{\text{p}})$, with $Z_{\text{p}} = 2$ and $u_{\text{p}} = 1.5$. These figures illustrate a fairly sensitive resolution of Z_{eff}. The marginal probability distribution for Z_{eff} (summed over u_0) is shown in Fig. 10. Clearly, the lack of precise knowledge of u_0 is no particular hindrance in resolving Z_{eff}. As we have seen previously (e.g. in Fig. 6), the resolution of u_0 can be accomplished quite finely.

In Fig. 9, the viewing is perpendicular, i.e. $\theta = 0$. One might question whether this

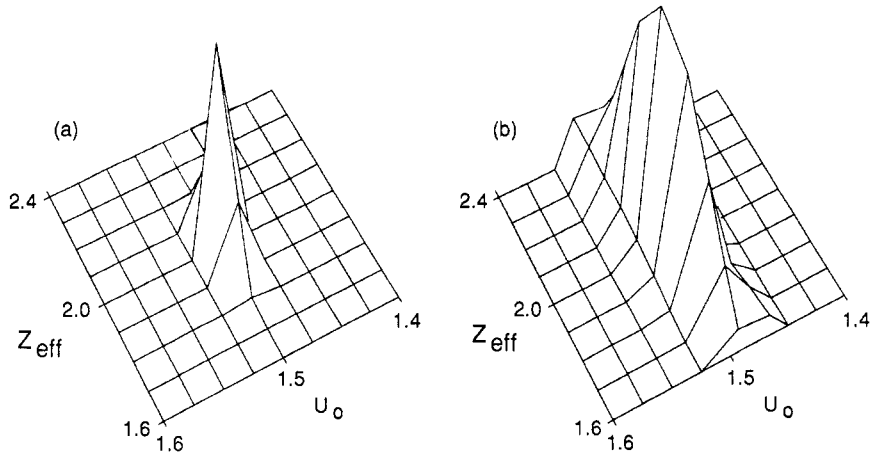

FIG. 9.—Joint probability distribution of Z_{eff} and u_0 for two noise levels: (a) $P(Z_{eff}, u_0 | Z_p = 2, u_p = 1.5; \sigma = 0.1)$ vs Z_{eff} and u_0, (b) $P(Z_{eff}, u_0 | Z_p = 2, u_p = 1.5; \sigma = 0.4)$ vs Z_{eff} and u_0. $\Delta u_0 = 0.3$. Polarization is ordinary. Viewing is at $\theta = 0°$. Here, $N_R = 80$ and $N_D = 1600$. A total of 81 cases was considered with $Z_{eff} = 1.6$–2.4 by 0.1, and $u_0 = 1.4$–1.6 by 0.025.

is the optimal viewing for distinguishing Z_{eff}; perhaps θ, a parameter over which we might exercise some control, might be chosen optimally with respect to distinguishing Z_{eff}. In fact, it might be surmised that viewing at a large angle would be particularly helpful. This might be because the main effect of different ion charge states is to isotropize at different rates the incremental electron distribution, and the Doppler-shifted radiation might highlight this pitch-angle scattering. In Fig 11, we compare the probability distribution of Z_{eff} for different viewing angles; here, we assume only Z_{eff} unknown, and we consider radiation viewed either perpendicularly or at 45°.

Note that there is some advantage in viewing at 45°; this we depict in different ways in Fig. 12. In Fig. 12a, we show for $Z_p = 2$ and for each of the two angles the probability as a function of noise of correctly deducing $Z_{eff} = 2$ (from the 11 *a priori* equally likely possibilities {1.5–2.5 in increments of 0.1}). Note that the correct charge state is more probable when viewed at the larger angle.

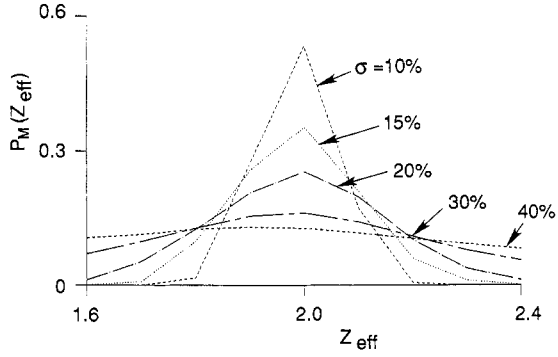

FIG. 10.—Marginal probability distribution $P(Z_{eff} | Z_p = 2, u_p = 1.5; \sigma)$, as derived from Fig. 9.

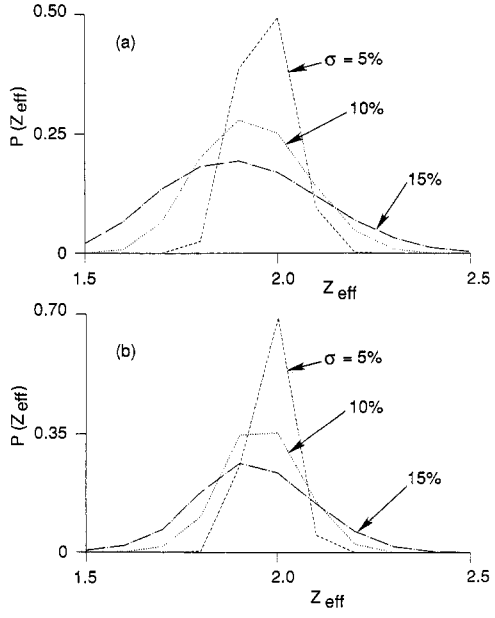

FIG. 11.—Probability distributions $P(\theta, Z_{\text{eff}}|Z_p = 2; \sigma)$ for different viewing angles: (a) $\theta \sim 0°$, (b) $\theta \sim 45°$. Noise levels are at $\sigma = 0.05$, $\sigma = 0.1$ and $\sigma = 0.15$. Here, $u_0 = 0.9$ and $\Delta u = 0.1$. Polarization is ordinary. The radiation is observed at 20 frequencies in the frequency window $2.2 < \omega/\omega_c < 2.6$. Here, $N_R = 80$ and $N_D = 800$.

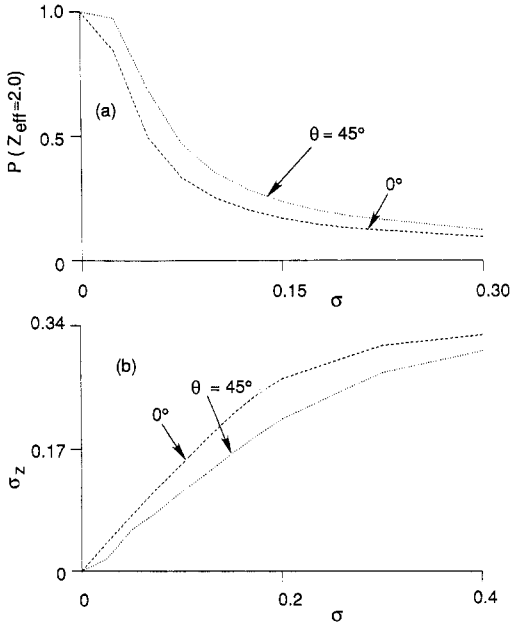

FIG. 12.—Distinguishing Z_{eff} at different angles. (a) $P(Z_{\text{eff}} = 2|Z_p = 2; \sigma)$ vs σ for $\theta = 0°$ and $\theta = 45°$, (b) σ_Z vs σ for $\theta = 0°$ and $\theta = 45°$. Other parameters same as in Fig. 11.

Figure 12b illustrates the characteristic deviation, σ_Z, of the probability distribution $P(Z_{\text{eff}}|Z_p = 2;\sigma)$ from the true charge state, Z_p, where σ_Z is defined by

$$\sigma_Z^2 \equiv \frac{1}{N}\sum_{i=1}^{N} P(Z_i|Z_p;\sigma)\,(Z_i - Z_p)^2. \tag{5.3}$$

Here, plotting σ_Z as a function of noise level σ, we can see that the characteristic deviation is indeed narrower for viewing at $\theta_p = 45°$. Note that σ_Z is not quite the standard deviation, since the mean of Z_i need not coincide with Z_p. Actually, this case, at either viewing angle, is an example where the maximum likelihood value of Z_{eff} clearly does not coincide with Z_p, although its deviation from Z_p is still small, and this deviation itself is also smaller for the observation at $\theta = 45°$ (see Fig. 11).

From Figs 11–12 it is evident that by viewing at $\theta_p = 45°$ rather than at $\theta_p = 0°$, it is possible to achieve the same resolution at about 50% higher noise levels. Moreover, the noise levels used in Figs 11–12 in comparing different viewing angles are the relative noise levels at each angle. In other words, in considering the radiation response for $\theta = 0°$, we polluted the data by noise chosen as a given fraction (σ) of the maximum amplitude of the radiation response $R(\omega, \tau;\ \theta = 0°)$. What we call the same noise for the case $\theta = 45°$ involves polluting the data by the same fraction of the maximum amplitude of the radiation response at $\theta = 45°$. So the comparison between viewing at the two angles is a reflection only of the distinguishing features of the radiation response, rather than the amplitude of the signal at different viewing angles.

Actually, it turns out that the signal viewed at $\theta = 45°$, in the frequency window that we employ (i.e. between the second and third harmonics), is about 50% larger than the signal viewed at $\theta = 0°$. This is because when viewed at such large angles, the Doppler-shifted second harmonic radiation appears in the same frequency window as, when viewed at $\theta = 0°$, does the relativistically downshifted third harmonic radiation. The lower harmonic radiation is greater than higher harmonic radiation, so, in addition to the increased resolution at $\theta = 45°$ that would be present at the same signal/noise ratio (as illustrated by Figs 11–12), there is an additional advantage in that the signal/noise ratio is likely to be greater at the oblique viewing angle.

It is of interest to identify other parameters, apart from the general viewing angle, over which we have some control, and whose values might be chosen in such a way as to optimize the sensitivity of the radiation response to an unknown parameter. A second parameter over which some control might be exercised (and through which a more sensitive radiation response might be constructed) is the impulse velocity locale u_0. Of course, the viewing window itself—the range in ω in which we place our detectors—might also highlight certain parameters, as might a particular polarization of the emission.

6. DEDUCING THE q-PROFILE

The parameter θ gives information on the q-profile, where q is defined by

$$q \equiv \frac{RB_p}{aB_T} = \frac{R}{a}\tan\beta, \tag{6.1}$$

and where β is the angle by which the magnetic field deviates from the toroidal direction. Here, R is the Tokamak major radius and a is the minor radius of the Tokamak at which the viewing takes place. It is the angle β that we wish to discover. Now we know how to view the plasma purely vertically, which is equivalent to viewing at an angle β with respect to the total magnetic field. More generally, we can deviate from purely perpendicular viewing by viewing at some known angle ϕ along the toroidal direction and in the plane that includes the vertical direction (see Fig. 13). The viewing angle with respect to the magnetic field, i.e. θ, is then given by

$$\theta = \beta + \phi. \tag{6.2}$$

Thus, by deducing θ, we arrive at β, since ϕ is known. Clearly, to the extent that θ is uncertain, i.e. $\Delta\theta$, so is β uncertain, i.e. $\Delta\theta = \Delta\beta$. Now the uncertainty in q, what we call Δq, is related to the uncertainty in β by

$$\Delta q = \frac{R}{a} \sec^2 \beta \Delta\beta, \tag{6.3}$$

from which derive the relations

$$\frac{\Delta q}{q} = \frac{1}{q}\frac{R}{a}\sec^2\beta\Delta\theta = \frac{1}{\sin\beta\cos\beta}\Delta\theta. \tag{6.4}$$

For most cases of interest, we may approximate $\sec^2 \beta \simeq 1$, so that $\Delta q/q = (R/qa)\Delta\theta$. Suppose that the resolution of θ is limited by an optical system beam divergence to $\Delta\theta \simeq 2^\circ \simeq 1/30$ radians, then $\Delta q/q \simeq 0.03(R/qa)$. There is particular interest, say, in knowing q near the $q = 1$ surface, near which we might have $R/a = 10$, which gives q to about 30%. For larger q, we also expect larger R/a; e.g. if near the $q = 1.5$ surface, we have $R/a = 5$, then we deduce q to about 10%.

For optical systems that are diffraction limited, we are (using the Rayleigh criterion) limited to

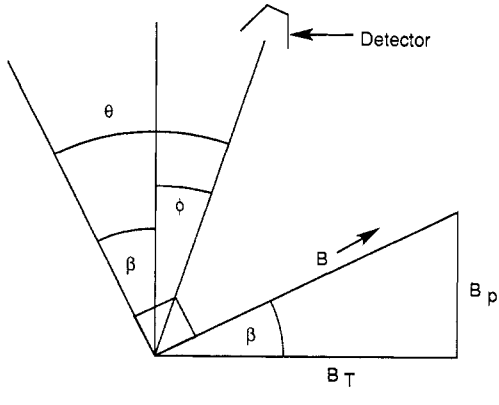

FIG. 13.—Deducing the q-profile.

$$\Delta\theta \geqslant 1.22\lambda/d, \tag{6.5}$$

where λ is the observed wavelength and d is the detector width. At 300 GHz, $\lambda \simeq 1$ mm, so that for $d = 30$ mm, we have $\Delta\theta \simeq 2°$. Observing at higher frequencies gives greater resolution. If the resolution of the viewing angle were not diffraction limited, the resolution would then be limited by noise, and the analysis of Section 5 pertains. In, principle, then, resolution to within a half degree might be had, as in Fig. 4 or Fig. 7. In this example, then, the resolution of $\Delta q/q$ would be four times sharper.

Note that synchrotron emission from the bulk plasma falls off rapidly for higher harmonics, but the incremental emission, which arises from mildly relativistic tail electrons, is relatively strong at the higher frequencies. Also, there may be an advantage here in the signal/noise ratio in viewing at oblique angles (note that $\Delta q/q$ is independent of ϕ) as there was in the case of distinguishing Z_{eff}. Of course, the need for narrow beam divergence in the optical system would be obviated were the stimulus for the incremental radiation itself narrowly focused, although that might be difficult in practice.

7. SUMMARY AND CONCLUSIONS

The invasive technique examined in this paper for utilizing transient, as opposed to steady, synchrotron radiation permits a very much more precise deduction of plasma parameters, even though the amount of processible information itself is not changed by the choice of examining a transient response. What has changed is that instead of relating the information obtained at each moment in time to the distribution at each moment, we relate all the information obtained over many moments to the state of the plasma at one moment. Were it necessary to track on a collisional time scale the parameters that govern the transient response, there would be no clear advantage to the latter scheme; however, when these parameters do change slowly, the kind of information gathered here does, in fact, allow a great deal more to be said about these parameters.

The transient response is arranged to be the response to a perturbation in the high-velocity, superthermal electron distribution function. The choice of perturbing very fast electrons is for several reasons. First, the dynamics of fast electrons are well established. Second, these electrons synchrotron radiate most copiously. Third, these electrons slow down most slowly, so that there is time enough to gather many independent time points in the radiation pattern $R(\omega, \tau)$. Fourth, in calculating the collisional scattering of superthermal electrons, energy drag dominates over energy diffusion; this enormously simplifies the theoretical analysis of the data, since, fortuitously, the characteristic equations that govern the response equations can be integrated analytically. We consider these reasons now in greater detail.

The first of these reasons, the established dynamics of fast electrons, is critical to the analysis—only by attempting to describe a clear, physical process, over which there is little disputation concerning the governing physics, can we make strong statements about the values parameters can take on the basis of any deviations from our expectations in an experiment. The physics of high-energy electrons is among the simplest of Tokamak plasma processes. The governing equations involve motion along field lines subject to the dual forces of coulomb collisions and d.c. parallel electric fields. Any narrow-band spectrum of high frequency waves can act only in a diffusive

capacity, and so such a spectrum, were it present, would not materially affect the electron orbits arising from a consideration only of the above directed forces. This assertion is expected to hold even were this spectrum of the type that might be used to perturb these electrons in the first place. Moreover, although there may be a variety of low-frequency fluctuations that affect slower electrons, these fast electrons are relatively immune to the turbulent processes that affect plasma transport. In fact, in the high-velocity limit, even the plasma temperature does not significantly affect the evolution of these electrons. The physical picture does become somewhat murky if there are not good magnetic surfaces, i.e. not good enough to confine the fast, perturbed electrons on the collisional time scale. In such an event, the analysis here would be limited to where the surfaces are good; elsewhere, our model may need improvement.

It is worthwhile to inquire into experimental evidence for the applicability of the collisional model, and, in particular, the applicability of this model with regard to fast electrons. The balance between the forces of collisions and the electric field gives rise to Spitzer conductivity, for which clearly there is ample evidence. This evidence does not, however, support directly the collisional model employed here, because conductivity arises largely from the motion of thermal, rather than superthermal, electrons. Also there are notable exceptions to the theoretical value of the conductivity, generally arising from the turbulence that affects the thermal, current-carrying electrons. More relevant as justification for the collisional model as applied here, where emphasis is placed on the very fast electrons, especially those initially with large parallel energy, is the very extensive series of current-drive and current ramp-up experiments on the PLT Tokamak (JOBES *et al.*, 1985). These experiments furnish perhaps the clearest evidence for the Coulomb collisional model for energetic electrons in a Tokamak; over a wide range of conditions these experiments were consistent to minute detail with the collisional model assumed here (FISCH and KARNEY, 1985; KARNEY *et al.*, 1985). Similar experiments performed on the ASDEX Tokamak (LEUTERER *et al.*, 1985) and on the Alcator C Tokamak (TAKASE *et al.*, 1987) offer further evidence for the wide applicability of this model. Note, however, that the physical model evidenced in these experiments concerns only Tokamak-averaged quantities; here, there is a further, but quite reasonable, assumption that the model is applicable on each flux surface.

The second and third reasons for employing fast electrons are a matter of signal enhancement. Apart from the copious emission of fast electrons, or the longer time with which to collect their radiation signal as they slow down, there may be further means to enhance the signal strength. For example, viewing at a finite angle ($\theta \neq 0$) may mean capturing a larger signal. Also, because of the relatively larger Doppler shift in the incremental radiation, viewing at a finite angle may mean that the background plasma presents a less confusing background signal.

The fourth advantage of using high-velocity electrons pertains to the kind of analysis that can be performed easily. The fact that the radiation equations in this limit are analytically solvable makes tractable a kind of data reduction that is often too difficult; rather than identifying merely a set of parameters which produces a good fit to data, we are enabled to examine a very complete set of parameters in order to obtain a probability distribution over parameter space.

What we have established here is that the incremental radiation response to brief

heating of fast electrons indeed reflects sensitively on certain plasma parameters of interest. Our study, however, is preliminary in nature. What we have not examined here is the means of producing the heating stimulus. Also, we have studied only the case of steady-state plasma, i.e. no d.c. electric field. In fact, it might be surmised that the plasma parameter for which a diagnostic based upon incremental radiation is particularly suitable is the plasma d.c. parallel electric field. This important parameter, which is very difficult to measure directly by any other means, is likely to be deducible through its acceleration of high velocity electrons. The question of plasma tomography is also not considered here; our purview was limited to the case of examining incremental radiation emanating from one location only in the plasma. These issues with which we have not dealt here present no conceptual difficulties, but do require a more complete and detailed treatment. What the present study has provided is the motivation for further study of what may be a promising diagnostic.

Acknowledgements—It is a pleasure to acknowledge useful discussions with Drs P. EFTHIMION and T. LUCE. This work was supported by the United States Department of Energy under contract numbers DE-AC02-76-CHO3073 and DE-FG02-84-ER53187.

REFERENCES

ALIKAEV V. V., BOBROVSKII G. A., POZNYAK V. I., RAZUMOV K. A., SANNIKOV V. V., SOKOLOV YU. A. and SHMARIN A. A. (1976) *Fiz. Plazmy* **2**, 390.

BORNATICI M., CANO R., DE BARBIERI O. and ENGLEMANN F. (1983) *Nucl. Fusion* **23**, 1153.

CELATA C. M. (1985) *Nucl. Fusion* **25**, 35.

CELATA C. M. and BOYD D. (1977) *Nucl. Fusion* **17**, 735.

FISCH N. J. (1987) *Rev. Mod. Phys.* **59**, 175.

FISCH N. J. (1988) *Plasma Phys. contr. Fusion* **30**, 1059.

FISCH N. J. and KARNEY C. F. F. (1985) *Phys. Rev. Lett.* **54**, 897.

GIRUZZI G. (1988) *Nucl. Fusion* **28**, 1413.

GIRUZZI G., FIDONE I., GRANATA G. and KRIVENSKI V. (1986) *Nucl. Fusion* **26**, 662.

HUCHINSON I. H. and KATO K. (1986) *Nucl. Fusion* **26**, 179.

JOBES F. C., BERNABEI S., CHU T. K., HOOKE W. M., MERSERVEY E. B., MOTLEY R. W., STEVENS J. E. and VON GOELER S. (1985) *Phys. Rev. Lett.* **55**, 1295.

KARNEY C. F. F., FISCH N. J. and JOBES F. C. (1985) *Phys. Rev. A* **32**, 2554.

KATO K. and HUCHINSON I. H. (1986) *Phys. Rev. Lett.* **56**, 340.

LANDAU L. D. and LIFSHITZ E. M. (1951) *Classical Theory of Fields*. Addison Wesley, Reading, MA.

LEUTERER F., ECKHARTT D., SÖLDNER F., BECKER G., BRAMBILLA M., BRINKSCHULTE H., DERFLER H., DITTE U., EBERHAGEN A., FUSSMANN G., GEHRE O., GERNHARDT J., GIERKE G. V., GLOCK E., GRUBER O., HASS G., HESSE M., JANESCHITZ G., KARGER F., KEILHACKER M., KISSEL S., KLÜBER O., KORNHERR M., LISITANO G., MAGNE R., MAYER H. M., MCCORMICK K., MEISEL D., MERTENS V., MÜLLER E. R., MÜNICH M., MURMANN H., POSCHENRIEDER W., RAPP H., RYTER F., SCHMITTER K. H., SCHNEIDER F., SILLER G., SMEULDERS P., STEUER K. H., VIEN T., WAGNER F., WOYNA, F. V. and ZOUHAR M. (1985) *Phys. Rev. Lett.* **55**, 75.

LUCE T., EFTHIMION P. and FISCH N. J. (1988) *Rev. Scient. Instrum.* **59**, 1593.

MAHAJAN S. M., OBERMAN C. and DAVIDSON R. C. (1974) *Plasma Phys.* **16**, 1147.

TAKASE Y., KNOWLTON S. and PORKOLAB M. (1987) *Physics Fluids* **30**, 1169.

TAMOR S. (1979) *Nucl. Fusion* **19**, 455.